2016

Assessing Defrosting Performance on Hydrophilic, Hydrophobic, and Micro-Patterned Heat Transfer Surfaces

Nickolas C. Schmiesing
Miami University, Oxford, OH, United States of America, schmienc@miamioh.edu

Andrew D. Sommers
Miami University, Oxford, OH, United States of America, sommerad@miamioh.edu

Assessing Defrosting Performance on Hydrophilic, Hydrophobic, and Micro-Patterned Heat Transfer Surfaces

Nickolas C. SCHMIESING[1], Andrew D. SOMMERS[1,*]

[1] Dept. of Mechanical and Manufacturing Engineering, Miami University, Oxford, OH 45056 USA
Phone: (513) 529-0718, Fax: (513) 529-0717, E-mail: sommerad@miamioh.edu

* Corresponding Author

ABSTRACT

In this work, differences in drainage rates and defrosting effectiveness were explored for surfaces of differing wettability. Both patterned and non-patterned surfaces were explored. To date, six surfaces have been examined—an uncoated, untreated aluminum plate (Sample 1), an identical plate treated with a hydrophilic coating (Sample 2), a plate containing evenly-spaced micro-channels with no surface coating (Sample 3), a plate containing evenly-spaced micro-channels with a hydrophobic coating (Sample 4), and a surface containing a microstructural roughness gradient both with and without a hydrophobic surface coating (Samples 5 and 6). Cyclical tests containing frosting periods and defrosting periods were conducted on each sample. Each cycle consisted of one hour of frost growth, followed by ten minutes of defrost and drainage. For these experiments, the frost layer was grown inside a Plexiglas environmental test chamber where the relative humidity was held constant (i.e. 60%, 80%) for the duration of the experiment using an ultrasonic humidifier. The temperature of the ambient air inside the enclosure was recorded to ensure that it remained constant throughout the experiment, and the surface temperature of the plate was fixed using a thermoelectric cooler (TEC). The TEC unit was placed on an electronic balance within the test chamber which permitted the frost mass to be recorded continuously during testing.

Overall, the surface defrosting effectiveness varied from 52-77% across all surfaces depending on the test conditions, with one test showing slightly lower percentages. Our data show that only small differences were observed in the defrosting effectiveness between the samples. The gradient surfaces however did remove slightly more water from the surface during defrosting (as compared to the baseline) when the frost was grown at colder surface temperatures. The average increase in defrosting effectiveness at T_w = -12°C was 2-4% for Surface 6 versus Surface 1. Interestingly, when the frost was grown at warmer surface temperatures, the gradient surfaces did not perform as well. In almost all cases, however, the defrosting effectiveness increased as the surface temperature was decreased during the frost growth period. This finding suggests that defrosting effectiveness is intrinsically linked to the thermophysical properties of the grown frost layer. Additional research is needed to investigate this phenomenon more fully. The overall aim of this work is to study the effects of surface wettability and micro-structural roughness on the defrosting performance of functionalized heat transfer surfaces.

1. INTRODUCTION

The study of frost formation and frost properties on surfaces remains an important consideration when designing new frost-tolerant heat exchangers and systems. In most cases, frost formation is undesirable because it forms a thermal barrier on the heat exchanger surface due to its porous structure and low overall thermal conductivity. As a result, frost growth typically reduces the heat transfer rate and can block the flow of air through the heat exchanger thereby degrading its performance. Moreover, most refrigerator evaporators require periodic defrosting which further increases their inefficiency due to this periodic downtime. And while super-hydrophilic and super-hydrophobic surfaces have been studied extensively in other contexts, relatively few papers could be found which have examined the influence of surface wettability on a growing frost layer. Moreover, most correlations ignore surface wettability when seeking to predict frost density on metallic surfaces. Thus, the development of more accurate frost growth and densification models represents an important issue for the HVAC&R industry; however, it is also expected that this research would benefit the aerospace and automotive industries where these models might be used to help mitigate surface drag, improve wing de-icing, etc.

Over the years, numerous frost studies and frost growth models have been published. For example, O'Neal and Tree (1984), Padki et al. (1989), and Iragorry et al. (2004) have each performed a critical review of the literature and tried to summarize the effect that various environmental parameters have on frost properties and frost growth models. Östin and Andersson (1991) concluded that the plate surface temperature and the air relative humidity both affect frost thickness; whereas, the density of the frost largely depends on the air velocity and to a lesser extent on the relative humidity. They also examined the contribution of the mass flux of condensed water vapor to frost density and frost thickness and found that the water vapor contributes nearly equally to increasing the frost density and frost thickness. Other seminal works include Hayashi et al. (1977) who derived a correlation to calculate the frost density, and Brian et al. (1970) who developed a correlation for calculating the effective thermal conductivity of the frost layer based on the mean frost surface temperature and the average frost density. Papers focused on the prediction of frost properties on conventional surfaces (esp. thermal conductivity) include Tokura et al. (1983), Yang and Lee (2004), Yang et al. (2004), Yonko and Sepsy (1967), and Lee et al. (1997).

One of the best recent works that was found on frost layer densification is by Hermes et al. (2014). In this work, the authors presented a first-principles based model for predicting the time-evolving porosity of a frost layer. This theoretical model was then combined with experimental data to produce a semi-empirical correlation for frost layer densification as a function of time and the modified Jakob number. It is also worth noting that the model by Hermes et al. (2014) was independent of the frost surface temperature while still providing an explicit relationship between frost density and time. Other papers on frost growth and densification include El Cheikh and Jacobi (2014), Cheng and Cheng (2001), Tao et al. (1993), Yun et al. (2002), LeGall and Grillot (1997), and Kandula (2011).

With regards to the influence of surface wettability on frost properties and defrosting behavior, only a few papers were found which address the subject. In a paper by Shin et al. (2003), three different surfaces having advancing dynamic contact angles (DCA) of 23°, 55°, and 88° were installed in a wind tunnel and exposed to a humid air flow. They found that during the initial period of frost formation, the shape of the micro droplets depended upon the surface energy, and the process of frost growth was affected by the advancing DCA. High DCA surfaces showed the presence of irregular and rough crystals during the initial period of frost deposition, which resulted in high frost thickness and low frost density, whereas low DCA surfaces produced low frost thickness and high frost density. This suggests that the growth of crystals is strictly controlled by surface energy during the early stages of frost growth. In a follow-up paper by the same group, Lee et al. (2004) studied the surfaces having dynamic contact angles of 23° and 88° in more detail. Frost structures were classified and frost maps were proposed. It was found that the lower DCA surface at lower humidity levels produced a denser frost due to a shifting in surface structure formation type. Overall, at low humidity, the frost structure is less porous and may be classified as plate-type, whereas at high humidity and low temperature, a very porous, feather-like frost structure is formed. This work also reported that while frost structure is primarily dependent on the humidity and plate temperature, frost density is affected by the air velocity. This would seem to imply that the influence of surface wettability may be more pronounced under natural convection conditions. Hoke et al. (2004) examined surfaces that were both hydrophilic and hydrophobic and discussed the effect of surface wettability and its impact on condensate distribution (the initial condition for frost growth). Interestingly, recent papers such as Liu et al. (2008), Wang et al. (2015), Fang and Amirfazli (2014), and Cai et al. (2011) have shown that super-hydrophobic surfaces may be able to restrain frost growth on the surface due to the high energy barrier for frost crystal nucleation on these surfaces. Delayed frosting times of as long as 55-60 minutes have been reported. This delay has been attributed at least in part to the nano-texture of super-hydrophobic surfaces which creates a large number of air pockets on the surface which exhibits an insulating behavior and results in a decrease in droplet surface contact area (Tourkine et al., 2009). In a related work by Huang et al. (2012), the effect of the contact angle on the water droplet freezing process was studied. Their results show that the contact angle has a direct influence on both the water droplet freezing time and frost crystal growth velocity.

Papers concerned with defrosting behavior and the influence of surface contact angle were even harder to find. Kim and Lee (2011) investigated the effect of fin surface contact angle on the frosting/defrosting performance of a heat pump under winter operating conditions. Static contact angles of 2.5°, 75°, and 142° were examined. On the hydrophobic surface, frost retardation was observed but the effect was not significant. The degree of super-cooling required for the onset of frost nucleation was also affected by the hydrophobic surface treatment. In comparison, the frost layer on the hydrophilic fin was thinner and had a greater average density. Overall, the effect of surface contact angle on the defrosting time however was found to be insignificant. In Rahimi (2015), incipient ice formation was studied on aluminum surfaces with different chemical modifications (i.e. PEG and PFOS) and nano-roughness. It was found that at the initial stage of ice formation, flat hydrophobic surfaces exhibit the lowest ice formation rate,

the smallest thickness and the highest ice density. Faster ice formation and lower ice density were observed on the untreated aluminum. This was attributed to the highly heterogeneous nature of the bare aluminum surface, leading to a broad distribution of surface energies on the microscopic scale. In turn, this results in the nucleation of widely separated water droplets/ice crystals on the high-energy nucleation centers for even minor sub-cooling and the formation of low-density feather-like ice structures. In another study, Kulinich et al. (2011) showed that super-hydrophobic surfaces are also not always ice-repellent and that the ice-repellent properties of super-hydrophobic materials can deteriorate during icing/deicing cycles due to damage to the surface asperities. They also showed that the anti-icing efficiency of super-hydrophobic surfaces is significantly lower in a humid atmosphere due to increased ice adhesion strength. In Janssen et al. (2012), a high-magnification imaging technique was described for quantifying frosting and defrosting behavior on surfaces. In addition to the improved accuracy, the authors report that the new method makes possible the rapid calculation of droplet geometry during defrosting events. In another paper by the same group, an analytical model for the frost melting process is described (Mohs and Kulacki, 2011).

Although it is well-known that surface wettability can affect the properties of a growing frost layer, very few papers were found in the open literature which discuss the influence of surface wettability on defrosting behavior and defrosting effectiveness. For those papers that were found, the range of applicability is often quite limiting. Furthermore, metrics for comparing the defrosting performance of surfaces over different defrosting times and conditions were found to be lacking (aside from the routine reporting of defrosting percentage). This highlights the need for additional study and the development of new predictive tools for assessing the defrosting performance of surfaces. In this work, differences in drainage rates and defrosting behavior were explored for both patterned and non-patterned surfaces with an emphasis placed on assessing performance variations over multiple frosting/defrosting cycles. A new metric for assessing defrosting performance was also presented.

2. EXPERIMENTAL METHOD

2.1 Test Surfaces / Data Collection

In this study, frosting/defrosting experiments were performed with the purpose of assessing the defrosting performance of the surface and issues related to multiple frost/defrost events. During these tests, the surface temperature was prescribed using a thermoelectric cooler (TEC). The air temperature and relative humidity were also recorded during each test and held constant using cool mist ultrasonic humidification. Each test lasted three hours and thirty minutes and consisted of three one-hour frost growth periods each followed by a ten minute defrosting period (i.e. three cycles). The test samples were constructed from aluminum alloy 5052 polished on one side to a brushed finish. The test surfaces all had the same dimensions and were approximately 99.5 mm × 80.2 mm × 3.4 mm in size. Details about the various plates and their differences in surface structure can be found in Table 1. Some of these surfaces were engineered with uniformly spaced microchannels (i.e. 25μm wide, 100μm apart), while others were designed with a surface tension gradient (consisting of variably spaced microchannels) to help facilitate the movement of water to preferred locations on the surface as shown in Figs. 1 and 2. Surfaces 3-6 were prepared using a Minitech Mini-Mill 3 desktop micro-milling machine housed in our lab. Prior to testing, the surfaces were cleaned in an ultrasonic bath to remove any particulate matter and lubricant remaining from the machining process. Afterwards, they were rinsed in isopropyl alcohol, acetone, and finally deionized water. For the coated surfaces, the surface was then immersed in a silane solution for approximately 5-10 minutes and cured at 100°C for 30 minutes. The hydrophobic silane used in this study was trimethoxypropylsilane, and the hydrophilic silane was an amino silane (i.e. $C_8H_{22}N_2O_3Si$) and a sulfur silane (i.e. $C_{18}H_{42}O_6S_4Si_2$) prepared in a 3:2 molar ratio.

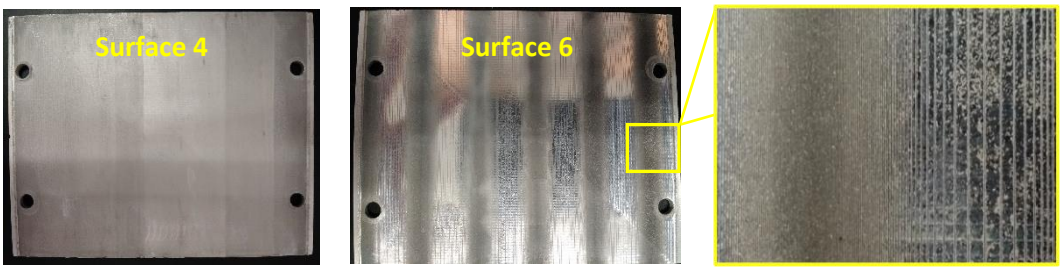

Figure 1: Pictures of the micro-milled test plates (Surfaces 4 and 6)

Table 1: Matrix of heat transfer test surfaces

No.	Material	Gradient?	Surface Features
1	Al	N	Baseline Surface
2	Al	N	Baseline Surface + Hydrophilic Silane Coating
3	Al	N	Uniform Channels (No Coating)
4	Al	N	Uniform Channels (w/ Hydrophobic Silane Coating)
5	Al	Y	Gradient Surface (No Coating)
6	Al	Y	Gradient Surface (w/ Hydrophobic Silane Coating)

2.2 Environmental Test Chamber

All experiments were performed in an environmental test chamber. To isolate the environmental conditions, a Plexiglas enclosure with a hinged, sealable lid was placed around the equipment as shown in Fig. 3. This Plexiglas enclosure had the dimensions 400.1mm × 257.2mm × 285.8mm. A Plexiglas partition was inserted vertically inside the box to create a front and rear chamber inside of the enclosure, thereby permitting higher relative humidities to be achieved near the sample and to help maintain a constant air temperature inside the front chamber. This partition was secured so as not to affect the balance. In order to control the temperature of the test samples, a thermoelectric cooler (A) was used. The test surface (B) was attached to the thermoelectric cooler (TEC). In order to minimize heat loss and prevent unwanted condensation, an insulating material was applied to the boundaries of the TEC. The lower edge of the test surface was left unobstructed in order to allow the frost melt to drain. During this melting process, the drainage was captured on a drip tray (C) located below the test surface. The drip tray prevented any melted frost from returning to the balance, thus allowing the total drainage mass to be determined. The mass of the frost growth was measured using a GP5202 Sartorius balance (D), which contained the thermoelectric cooler and the test surface. The frost mass was sampled and recorded at a frequency of approximately once every 10 seconds. The environmental conditions were monitored and recorded using an OMEGA OM-73 temperature/relative humidity data logger (E), while a set-point controller (F) was used to turn ON and OFF an ultrasonic cool mist humidifier which was connected to the test chamber through a sealed entrance tube (G). With this setup, the relative humidity inside the enclosure could be maintained to within ±2-3% of the set-point value, and the air temperature was typically held constant to within ±0.5ºC. T-type thermocouples were used to measure the plate and stage temperatures. The stage temperature was determined using two thermocouples affixed directly to the TEC surface by epoxy. The test plate temperature was determined using two thermocouples inserted into small holes drilled into the side of the test plates (one on each side). The depth of the holes was approx. 6-8 mm. Thermal paste was applied to the thermocouple junction before insertion, and epoxy was used to hold the thermocouple securely in place. The test plates were secured to the TEC stage using thermal paste and four Nylon screws with Teflon spacers to minimize water retention and thermal losses from the surface.

At the start of each test, the desired voltage was set for the TEC, and a thin plastic sheet was applied to the test surface to prevent condensation and/or frosting on the surface before the desired surface temperature was reached. Once the set-point temperature was reached, the plastic sheet was removed and the frost growth period was started. All tests were performed at constant voltage to the TEC. Three different plate surface temperatures (and their associated TEC voltages) were examined in this study—namely, -8°C (16VDC), -10°C (18.6VDC), and -12°C (22VDC). These represent typical steady-state values. Small differences (< 1°C) were observed from test to test. Tests were performed at either 60% RH or 80% RH and ambient air temperatures between 21-23°C. Conditions were fixed at the start of each experiment. (Note: The results shown here correspond to the 60% RH condition unless otherwise specifically noted.) In order to more fully examine the defrosting performance of the different surfaces, a testing method involving three cycles (1 hour frost, 10 minute defrost) was implemented. In total, each test lasted three hours and thirty minutes. Defrosting was initiated by turning ‘OFF’ the power to the TEC and allowing the stage to warm up to room temperature and melt the frost. The humidifier was also turned ‘OFF’ during this period to minimize any effect on the surface drainage process.

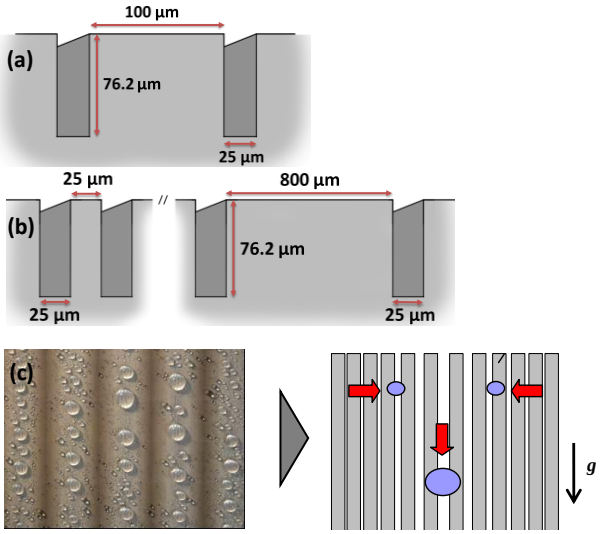

Figure 2: Images which illustrate the gradient concept on Surfaces 5-6: (a) uniform channels, (b) gradient geometry, (c) motivating idea with spray test on laser-etched surface

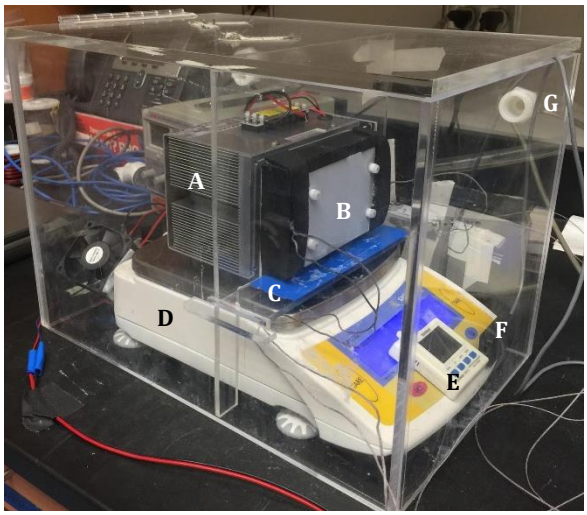

Figure 3: Environmental chamber used for the defrosting experiments showing the various components

3. RESULTS AND DISCUSSION

The results from the defrosting experiments are plotted in Fig. 4. Shown here is the defrosting efficiency (%) of the surface over three cycles for the six surfaces for the three examined surface temperatures (i.e. -8°C, -10°C, and -12 °C). These represent typical surface temperature values. Small differences (< 1°C) were observed from test to test. The relative humidity was maintained at 60% for these experiments. In this table, the "defrosting percentage" is defined as the ratio of drained water mass to the initial mass of frost on the surface prior to defrosting. A few observations are worth noting here. First, in almost all cases independent of the surface, the defrosting efficiency decreased from cycle to cycle with the lowest defrosting percentage generally associated with Cycle 3. In most cases, this degradation in defrosting efficiency was 5-10%. Thus, using the defrosting efficiency from the 1st cycle to predict future performance could lead to significant error. This also highlights the need in the literature for additional experimentation involving multiple defrosting events. Most published studies in the open literature today only examine one defrosting event (or a limited number of cycles). Second, differences between the various surfaces were generally small. This suggests that surface strategies that work well in a condensing environment for improved condensate management may not necessarily apply to a frosting environment with regards to improved defrosting performance. In other words, as might be expected, the behavior of a melting/draining frost layer is different from the behavior associated with the condensation of water droplets. Third, the defrosting efficiency for all surfaces generally increased as the surface temperature decreased. This is likely due to differences in the initial frost mass on the surface. Because more frost mass tends to accumulate on colder surfaces, it is thought that more droplets and/or larger droplets may form on these surfaces during melting thereby increasing the chances for "droplet sweeping" (i.e. the process by which a draining droplet will carry other droplets with it that are located underneath). Fourth, small but significant differences in individual surface performance were noted between the T_w = -8°C experiments and the T_w = -12°C experiments. At T_w = -8°C, Surface 3 (uniform microchannels) performed slightly better than the other surfaces including the baseline surface; whereas at T_w = -12°C, Surface 6 (gradient surface with coating) performed slightly better than the rest. It is believed that this may stem from small differences in the frost layer density and the overall ice crystal structure. For example, it is generally accepted that denser frost layers tend to form on warmer surfaces (as $T_w \rightarrow 0$°C) which means slightly higher frost thermal conductivity values exist on the T_w = -8°C surface. As a result, the frost may transfer heat more effectively in which case the uniform microchannels on Surface 3 facilitate an easier (and thus more efficient) removal of the frost layer. On the colder surface (i.e. T_w = -12°C), the frost is generally fluffier and is not as dense. Here, the "slower" melting of the frost layer may afford more opportunities for the coalescence of individual water droplets due to the underlying gradient pattern. At this time however, the exact reason for these differences is unknown.

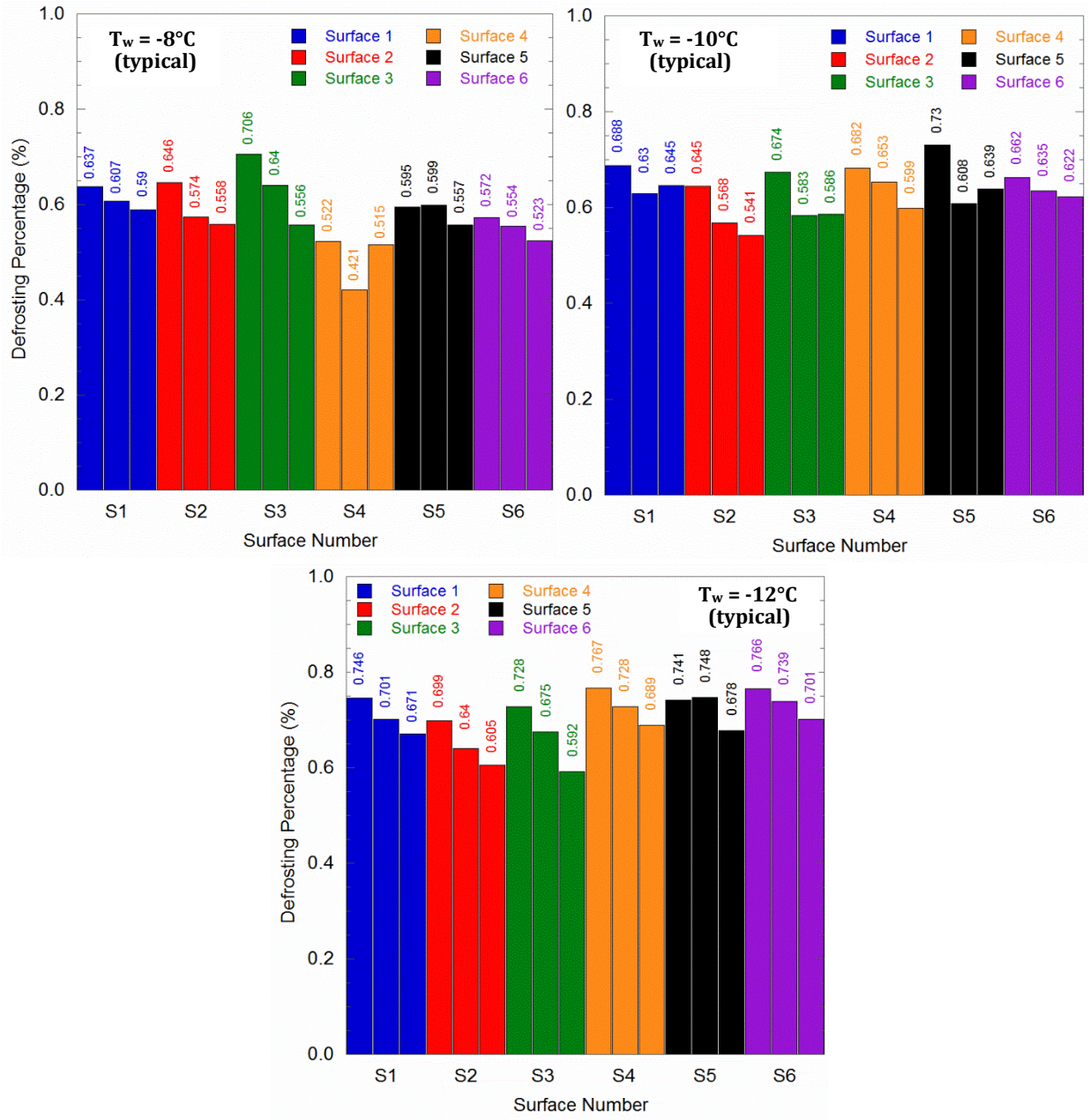

Figure 4: Defrosting efficiency (%) over three consecutive frosting/defrosting events for three different surface temperatures on Surfaces 1-6

Figs. 5 and 6 highlight the influences that both the air and plate surface temperatures have on the structure of the growing frost and its crystals. In Fig. 5, the impact of the surface temperature (i.e. T_w) on the frost density is presented by considering Kobayashi (1958)'s frost morphology map which predicts needle-like ice structures at warm surface temperatures (i.e. $T_w \approx$ -5°C) but sectorated plates at slightly colder temperatures (i.e. -20°C < T_w < -10°C) for slightly supersaturated air. The formation of these needle-like crystals at warmer surface temperature in turn leads to the denser frost layers that were mentioned earlier. The impact of air temperature on the structure of the frost can be seen below in Fig. 6. It is important to note that most frost studies have been performed at ambient temperatures above 0°C. In this work by Yamashita et al. (2007), two different growth stages were noted over the range -20°C < T_a < 0°C. At higher air temperatures, needle-like ice structures were observed that became the basis for a denser frost layer with time. At colder air temperatures, block-shaped structures were observed that could be seen to retain their structure

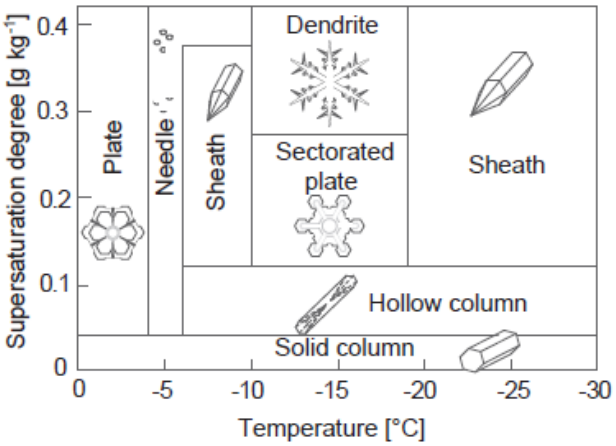

Fig. 5 Kobayashi (1958)'s frost morphology map as a function of the surface temperature (T_w) and supersaturation degree

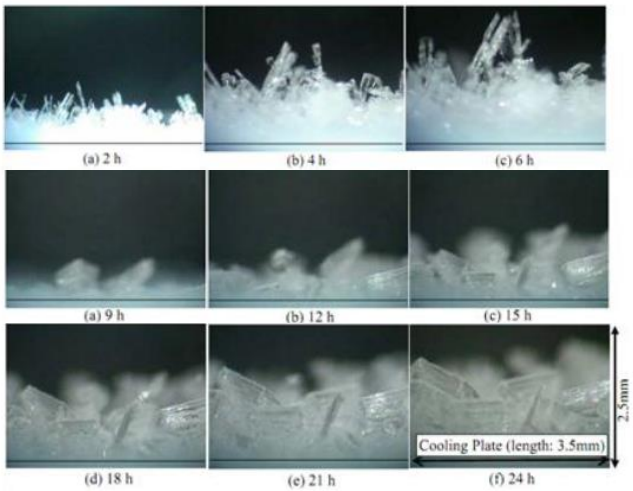

Fig. 6 Images of a frost layer showing different structures: (a) T_a = 0 to -5 °C, and (b) T_a = -10 to -20°C (Yamashita et al., 2007)

over long periods of time. These results suggest that the structure of the frost depends on the air temperature in a complex manner. In the present study, the frost was grown on the surface at approximately the same ambient air temperature for all tests. Thus, the influence of T_a on the frost structure is expected to be small.

Interesting differences were also observed with respect to the rate of frost deposition on the surface. As shown in Fig. 7, the rate of frost deposition on Surface 2 (hydrophilic coating) was noticeably higher than on Surface 3 (uniform channels). This was observed for all three examined surface temperatures and persisted after each defrosting event. This suggests that frost accumulation and blockage would likely be more severe on this surface and that the hydrophilic coating used on Surface 2 would likely result in shorter operational periods between defrosting if used on a heat exchanger. The rate of frost deposition on the surface was also linear with time and strongly dependent (as might be expected) with the surface temperature (i.e. T_w). Higher deposition rates were observed when the surface temperature was lower (i.e. -12°C vs. -7°C). Tests were also performed to check the overall repeatability of these experiments. This was performed on multiple surfaces and showed that these defrosting experiments are highly repeatable. Shown in Fig. 8 are the frosting and defrosting data for Surface 2 and 5. These tests were performed several days apart under the same operating conditions (i.e. RH = 80%, T_w = -13 to -14°C for Surface 2 and RH = 60%, T_w = -10 to -10.5°C for Surface 5).

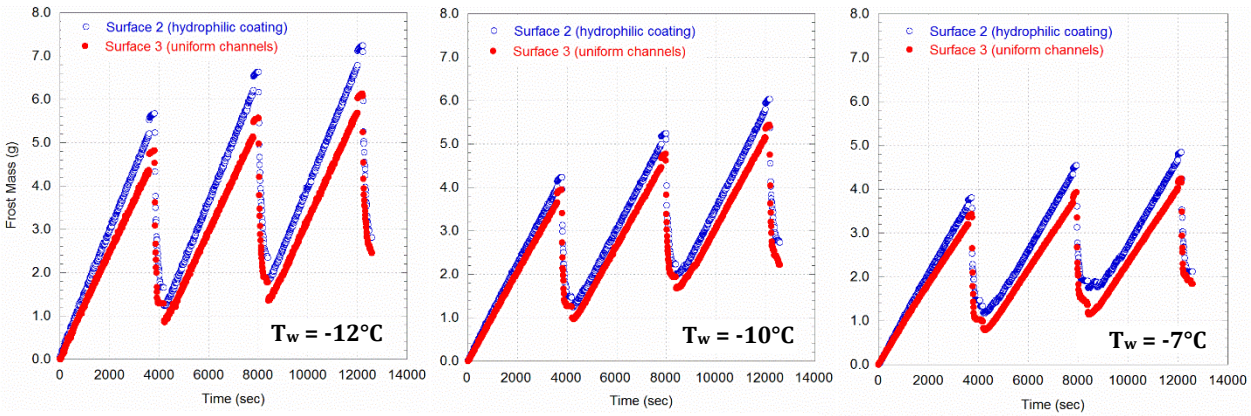

Figure 7: Rate of frost deposition on Surfaces 2 and 3. Higher deposition rates were consistently observed on Surface 2 and are attributed to presence of the hydrophilic silane coating.

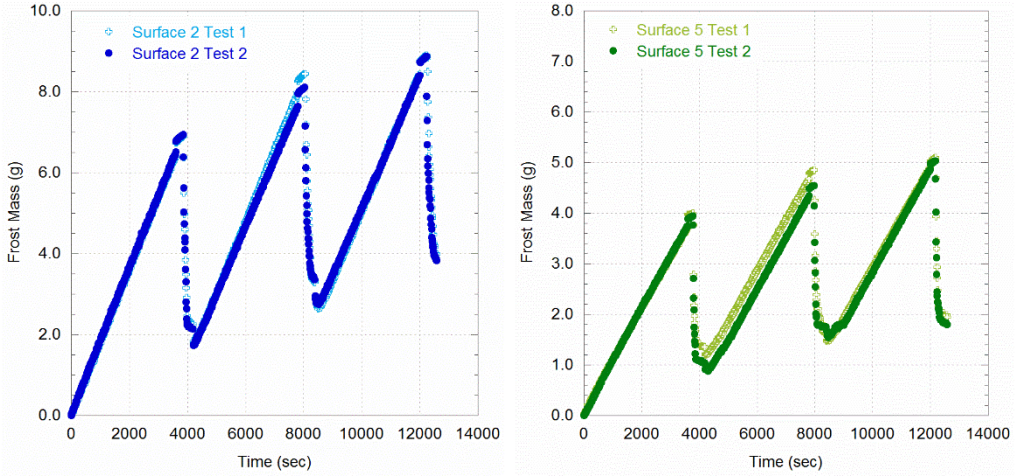

Figure 8: Repeatability tests to check for similar performance on Surface 2 and 5. Good repeatability was observed.

Overall, these tests revealed only small differences in the defrosting performance among the various surfaces. At lower surface temperatures, a small but significant improvement (i.e. 1-3%) was noted on the gradient surfaces (Surfaces 5-6) particularly in the later cycles (i.e. Cycles 2-3). These tests were performed at a fixed defrosting interval (60 min) and for a fixed defrosting period (10 min). If there were slight differences in either of these two parameters however (as is often the case in application), then this enhancement might have been lost. For this reason, we propose the use of another metric Φ for evaluating differences in surface performance.

$$\Phi = \left[\frac{(m_{\text{removed}}) \times (t_{\text{frost}})}{(t_{\text{defrost}}) \times (m_{\text{initial}})} \right] \tag{1}$$

This metric Φ (which is dimensionless) takes into account differences in the defrost time as well as differences in frosting time and the initial frost mass on the surface. This is important since surfaces with a higher initial frost mass might be expected to drain more water due to the higher gravitational forces experienced by the frost layer. In this case, as expected, the defrosting percentage and defrost metric Φ displayed similar trends. Another potential advantage of this metric is its ability to identify the surface's "optimal performance" early on the in the defrosting period. When conventional metrics (such as defrosting percentage) are used, the percentage is observed to continually increase with increasing defrosting time due to the ongoing periodic drainage of droplets from the surface and evaporation. This makes it difficult to compare individual surfaces when only a limited quantity of data are available. With the new metric, a local maximum is evident early in the defrosting period as shown in Fig. 9 and

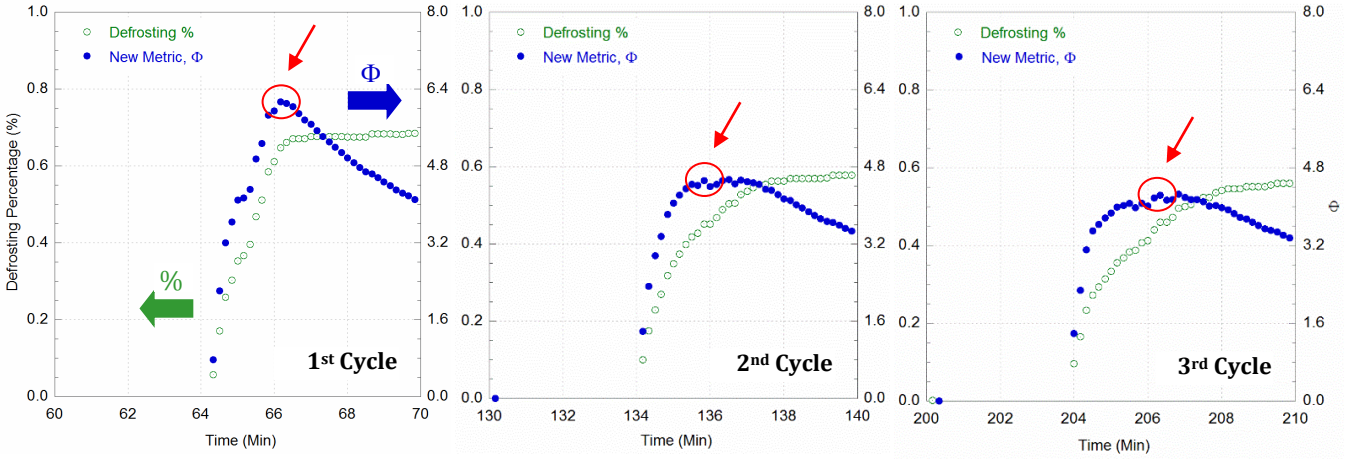

Figure 9: Comparison between the new defrosting metric Φ and defrosting percentage on Surface 2 at 80% RH

then is typically constant for a short time afterwards. A marked decrease in Φ after this period suggests that the surface is no longer removing an appreciable amount of water, and the defrosting cycle may be operating inefficiently now (i.e. $t_{defrost}$ is increasing with very little change in $m_{removed}$). In this figure, the maximum value of Φ typically occurred within two minutes after the onset of melting (i.e. Φ_{max} = **6.13** for Cycle 1, **4.53** for Cycle 2, and **4.25** for Cycle 3). This figure also suggests that about 6 minutes of defrosting is "optimal" in Cycle 1 before Φ starts to decrease, whereas in Cycle 2 and 3, approximately 7-8 minutes of defrosting is "optimal."

4. CONCLUSIONS

In this work, the defrosting performance of six different surfaces was analyzed to determine the effect that an underlying surface energy and/or wettability pattern had on the ability of that surface to drain water during the defrost cycle. Of particular interest was a roughness gradient surface pattern which was shown to facilitate the collection of water in preferred locations on the surface during spray tests.

Experiments consisting of three distinct frost/defrost cycles were performed on each surface. Each cycle consisted of one hour of frost growth, followed by ten minutes of defrost and drainage. Overall, the surface defrosting effectiveness varied from 52-77% across all surfaces depending on the test conditions, with one test showing slightly lower percentages. Our data show that only small differences were observed in the defrosting effectiveness between the samples. The gradient surface however did remove slightly more water during defrosting (as compared to the baseline) when the frost was grown at colder surface temperatures. The average increase in defrosting effectiveness at T_w = -12°C was 2-4% for Surface 6 versus Surface 1. When the frost was grown at warmer surface temperatures however, the gradient surface did not perform as well. Finally, defrosting effectiveness was observed to increase as the surface temperature was decreased during the frost growth period. This finding suggests that defrosting effectiveness is intrinsically linked to the thermophysical properties of the grown frost layer. Additional research is needed to investigate this more fully. A new metric for assessing defrosting performance was also presented.

NOMENCLATURE

A	heat transfer area	(m^2)	**Greek Symbols**	
CA	contact angle	(°)	δ	frost thickness (mm)
m	frost mass	(g)	Φ	defrosting metric
RH	relative humidity	(%)	**Subscripts**	
T	temperature	(°C)	a	air
t	time	(sec)	f	frost
V	voltage	(V)	w	wall surface

REFERENCES

O'Neal, D. L., and Tree, D. R., 1984, Measurement of Frost Growth and Density in a Parallel Plate Geometry, *ASHRAE Transactions*, vol. 90, no. 2A, pp. 278–290.

Padki, M. M., Sherif, S. A., and Nelson, R. M., 1989, A Simple Method for Modeling the Frost Formation Phenomenon in Different Geometries, *ASHRAE Transactions*, vol. 95, no. 2, pp. 1127–1137.

Iragorry, J., Tao, Y.-X., and Jia, S., 2004, A Critical Review of Properties and Models for Frost Formation Analysis, *HVAC&R Research*, vol. 10, no. 4, pp. 393-419.

Östin, R., Andersson, S., 1991, Frost growth parameters in a forced air stream, *Int. J. Heat Mass Trans.* 34, p. 1009-17.

Hayashi, Y., Auki, A., Adachi, S., Hori, K., 1977, Study of frost properties correlating with frost formation types, *J. Heat Transfer* 99, pp. 239-245.

Brian, P.L.T., Reid, R.C., Shah, Y.T., 1970, Frost deposition on cold surfaces, *Ind. Eng. Chem. Fund.* 9(3), p. 375-380.

Tokura, I., Saito, H., Kishinami, K., 1983, Study on properties and growth rate of frost layers on cold surfaces, *J. Heat Transfer* 105(4), pp. 895-901.

Yang, D.K., Lee, K.S., 2004, Dimensionless correlations of frost properties on a cold plate, *Int. J. Refrig.* 27, p. 89-96.

Yang, D.K., Lee, D.H., Kim, J.S., Lee, K.S., 2004, Modeling of frost behavior on a cold plate, *Proc. of the Int'l Refrig. and Air Conditioning Conference at Purdue*, West Lafayette, IN, July 12-15, Paper No. R121.

Yonko, J.D., Sepsy, S.F., 1967, An investigation of the thermal conductivity of frost while forming on a flat horizontal plate, *ASHRAE Transactions* 73(2), pp.1.1-1.11.

Lee, K.S., Kim, W.S., Lee, T.H., 1997, A one-dimensional model for frost formation on a cold flat surface, *Int. J. Heat Mass Transfer* 40(18), pp. 4359-4365.

Hermes, C.J.L., Loyola, F.R., Nascimento Jr., V.S., 2014, A semi-empirical correlation for the frost density, *Int. J. Refrig.* 46, pp. 100-104.

Yamashita, K., Hamada, M., Ise, S., Ohkubo, H., 2007, Study of frost properties in a low temperature environment, *22nd Int'l. Congress of Refrigeration*, Beijing, China, Paper No. ICR07-B2-809.

El Cheikh, A. Jacobi, A., 2014, A mathematical model for frost growth and densification on flat surfaces, *Int. J. Heat Mass Transfer* 77, pp. 604-611.

Cheng, C.-H., Cheng, Y.-C., 2001, Predictions of frost growth on a cold plate in atmospheric air, *Int. Comm. Heat Mass Transfer* 28(7), pp. 953-962.

Tao, Y.X., Besant, R.W., Rezkallah, K.S., 1993, A mathematical model for predicting the densification and growth of frost on a flat plate, *Int. J. Heat Mass Transfer* 36(2), pp. 353-363.

Yun, R., Kim, Y., and M. Min, 2002, Modeling of frost growth and frost properties with airflow over a flat plate, *Int. J. Refrig.* 25(3), pp. 362-371.

Le Gall, R., Grillot, J.M., 1997, Modeling of frost growth and densification, *Int. J. Heat Mass Transfer* 40(13), pp. 3177-3187.

Kandula, M., 2011, Correlation of water frost porosity in laminar flow over flat surfaces, *Special Top. Rev. Porous Media – Int. J.* 3, pp. 79-87.

Shin, J., Tikhonov, A.V., Kim, C., 2003, Experimental study on frost structure on surfaces with different hydrophilicity: density and thermal conductivity, *J. Heat Transfer* 125, pp. 84-94.

Lee, H., Shin, J., Ha, S., Choi, B., Lee, J., 2004, Frost formation on a plate with different surface hydrophilicity, *Int. J. Heat Mass Transfer* 47, pp. 4881-4893.

Hoke, J.L., Georgiadis, J.G., Jacobi, A.M., 2004, Effect of substrate wettability on frost properties, *J. Thermophysics and Heat Transfer* 18(2), pp. 228-235.

Liu, Z., Gou, Y., Wang, J., Cheng, S., 2008, Frost formation on a super-hydrophobic surface under natural convection conditions, *Int. J. Heat Mass Transfer* 51, pp. 5975-5982.

Wang, Z.-J., Kwon, D.-J., DeVries, K.L., Park, J.-M., 2015, Frost formation and anti-icing performance of a hydrophobic coating on aluminum, *Exp. Therm. Fluid Sci.* 60, pp. 132-137.

Fang, G., Amirfazli, A., 2014, Understanding the anti-icing behavior of superhydrophobic surfaces, *Surface Innovations* 2, pp. 94-102.

Cai, L., Wang, R., Hou, P., Zhang, X., 2011, Study on restraining frost growth at initial stage by hydrophobic coating and hygroscopic coating, *Energy and Buildings* 43, pp. 1159-1163.

Tourkine, P., Le Merrer, M., Quéré, D., 2009, Delayed freezing on water repellent materials, *Langmuir* 25(13), pp. 7214-7216.

Huang, L., Liu, Z., Liu, Y., Gou, Y., Wang, L., 2012, Effect of contact angle on water droplet freezing process on a cold flat surface, *Exp. Therm. Fluid Sci.* 40, pp. 74-80.

Kim, K., Lee, K.-S., 2011, Frosting and defrosting characteristics of a fin according to surface contact angle, *Int. J. Heat Mass Trans.* 54, pp. 2758-2764.

Kim, K., Lee, K.-S., 2011, Effects of surface treatment on frost formation and defrosting, *Proc. of the ASME/JSME 8th Thermal Engineering Joint Conference*, Honolulu, Hawaii, March 13-17, Paper No. AJTEC2011-44662.

Rahimi, M., Afshari, A., Fojan, P., Gurevich, L., 2015, The effect of surface modification on initial ice formation on aluminum surfaces, *Applied Surface Science* 355, pp. 327-333.

Kulinich, S.A., Farhadi, S., Nose, K., Du, X.W., 2011, Superhydrophobic surfaces: Are they really ice-repellent? *Langmuir* 27(1), pp.25-29.

Janssen, D.D., Mohs, W.F., Kulacki, F.A., 2012, High resolution imaging of frost melting, *Proc. of the ASME Summer Heat Transfer Conference*, Rio Grande, Puerto Rico, July 8-12, Paper No. HT2012-58061.

Mohs, W.F., Kulacki, F.A., 2011, Heat and mass transfer in the defrost process– a new modeling paradigm, *23rd IIR Int'l. Congress of Refrigeration*, Prague, Czech Republic, August 21-26, Paper No. 158.

Kobayashi, T., 1958, On the habit of snow crystals artificially produced at low pressures, *J. Met. Soc. Japan* 36, pp. 193-208.

ACKNOWLEDGEMENT

The authors gratefully acknowledge the involvement of Christian Petty, a recent Miami University graduate and current employee at Dayton Superior Corp., for his help and assistance during the early stages of this project.